AGU PUBLICATIONS

Geophysical Research Letters

RESEARCH LETTER
10.1002/2016GL069117

Key Points:
- Clarion-Clipperton fracture zone sediments are characterized by broad (meter-scale) suboxic zones
- Ammonium may provide additional reducing power in carbon-starved sediments
- Anaerobic ammonium oxidation may occur in the presence of manganese oxides in suboxic sediments

Supporting Information:
- Supporting Information S1

Correspondence to:
J. M. Mogollón,
j.m.mogollonlee@uu.nl

Citation:
Mogollón, J. M., K. Mewes, and S. Kasten (2016), Quantifying manganese and nitrogen cycle coupling in manganese-rich, organic carbon-starved marine sediments: Examples from the Clarion-Clipperton fracture zone, *Geophys. Res. Lett.*, *43*, 7114–7123, doi:10.1002/2016GL069117.

Received 13 APR 2016
Accepted 17 JUN 2016
Accepted article online 23 JUN 2016
Published online 9 JUL 2016

Quantifying manganese and nitrogen cycle coupling in manganese-rich, organic carbon-starved marine sediments: Examples from the Clarion-Clipperton fracture zone

José M. Mogollón[1,2], Konstantin Mewes[1], and Sabine Kasten[1]

[1] Alfred Wegener Institute Helmholtz Centre for Polar and Marine Research, Bremerhaven, Germany, [2]Now at Department of Earth Sciences-Geochemistry, Utrecht University, Utrecht, Netherlands

Abstract Extensive deep-sea sedimentary areas are characterized by low organic carbon contents and thus harbor suboxic sedimentary environments where secondary (autotrophic) redox cycling becomes important for microbial metabolic processes. Simulation results for three stations in the Eastern Equatorial Pacific with low organic carbon content (<0.5 dry wt %) and low sedimentation rates (10^{-1} – 10^{0} mm ky^{-1}) show that ammonium generated during organic matter degradation may act as a reducing agent for manganese oxides below the oxic zone. Likewise, at these sedimentary depths, dissolved reduced manganese may act as a reducing agent for oxidized nitrogen species. These manganese-coupled transformations provide a suboxic conversion pathway of ammonium and nitrate to dinitrogen. These manganese-nitrogen interactions further explain the presence and production of dissolved reduced manganese (up to tens of μ*M* concentration) in sediments with high nitrate (>20 μ*M*) concentrations.

1. Introduction

Deep-sea sediments occupy the largest areal extent of the global ocean basins, yet they receive the lowest amounts of organic carbon [*Dunne et al.*, 2007] and are thus characterized by deep oxygen penetration depths [*Fischer et al.*, 2009; *Røy et al.*, 2012]. Previous studies indicate that these areas may contain broad suboxic (absence of oxygen and sulfide) sedimentary zones (decimeter scale) [*D'Hondt et al.*, 2009; *Ziebis et al.*, 2012]. Suboxic zones favor geochemical reactions which contrast with those in anoxic-euxinic (no oxygen but sulfidic) or oxic settings. For example, the Gibbs free energy for ammonium oxidation through manganese oxides (Mn-anammox) is favorable [*Luther et al.*, 1997] but may be limited by low manganese oxide concentrations. Nevertheless, in locations such as the Clarion-Clipperton fracture zone (CCFZ), where high manganese oxide contents (>0.05 wt %) have been measured [*Mewes et al.*, 2014], the nitrogen and manganese cycles may be coupled.

Javanaud et al. [2011] demonstrated that isolated prokaryotes perform nitrification in anaerobic sediments containing high levels of manganese oxides. These authors theorized that the generated nitrate fueled additional denitrification and/or anaerobic ammonium oxidation with nitrite (anammox) [*Kuypers et al.*, 2003]. Their results followed previous field observations of nitrate peaks in anoxic sedimentary intervals [*Gingele and Kasten*, 1994; *Hulth et al.*, 1999; *Mortimer et al.*, 2004], typically occurring in manganese oxide-rich sediments. Furthermore, *Lin and Taillefert* [2014], via incubated sediments from a tidal salt marsh, revealed that manganese oxide-catalyzed anaerobic nitrification is an important consumer of ammonium in pore waters where sulfate reduction is absent (i.e., under suboxic conditions).

In this study, sedimentary profiles collected from the CCFZ, a manganese oxide-rich, organic carbon-poor environment [*Rühlemann et al.*, 2011; *Mewes et al.*, 2014], contain overlapping reduced and oxidized species of both nitrogen and manganese, which we posit to occur due to a coupling of the manganese and nitrogen cycles. This coupling involves both the oxidation of dissolved reduced manganese with nitrate [e.g., *Javanaud et al.*, 2011; *Lin and Taillefert*, 2014] and anammox aided by the presence of manganese oxides (Mn-anammox).

The CCFZ is located in the Northeastern Equatorial Pacific between the Clarion and the Clipperton fractures, which bound the area from the north and the south, respectively (Figure 1). It is located at water depths

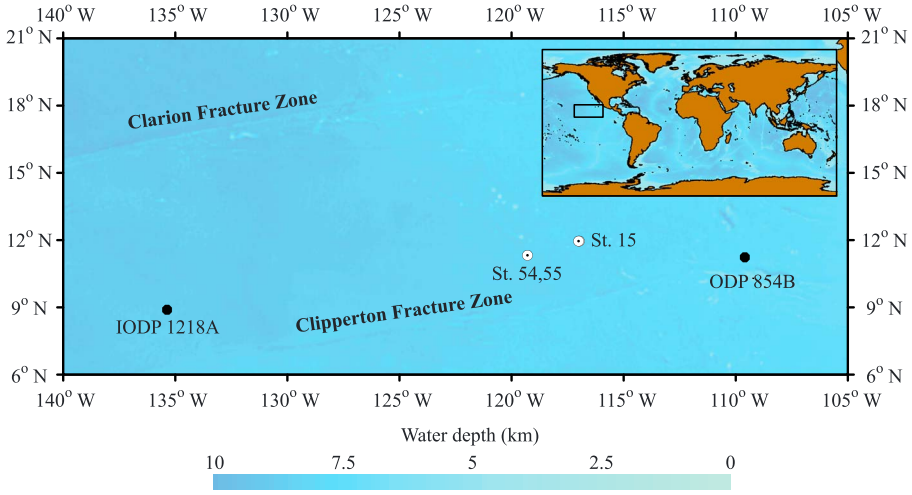

Figure 1. Study area with station (St.) locations (Bullseye), international drilling project stations (filled circles), and global location (insert). Note that at this scale Stations 54 and 55 overlap.

exceeding 3500 m and has a pronounced oxygen minimum zone 600–800 m thick, [*Wishner et al.*, 1995; *Zheng et al.*, 2000]. Organic matter delivery to the seafloor is low (up to 0.3 mol m^{-2} yr^{-1}), and the sediment surface often contains an abundance of (ferro)manganese nodules [*Murray and Kuivila*, 1990]. We investigate the sedimentary geochemical cycling at three stations (Station 15: latitude: 11.321°N, longitude: 119.287°W, water depth: 4366 m; Station 54: latitude: 11.954°N, longitude: 116.977°W, water depth: 4106 m; and Station 55, latitude: 11.954°N, longitude: 117.007°W, water depth: 4025 m) sampled in the CCFZ during RV *SONNE* cruise SO 205 in April/May 2010 [*Mewes et al.*, 2014]. These sites exhibit a sedimentary redox zonation with a prominent oxic zone (oxygen penetration depth, OPD, of ~2–4 m), and below, a pronounced suboxic zone with a thicknesses exceeding 10 m [*Mewes et al.*, 2014, Figure 2].

2. Methods

2.1. Sediment Sampling and Measurements

Sediment cores retrieved during RV *SONNE* cruise SO 205 in April/May 2010 [*Rühlemann et al.*, 2011] were transferred into the vessels and placed in a cold room (4°C) directly after recovery. Pore water was retrieved using a rhizons with an average pore diameter of 0.15 μm [*Seeberg-Elverfeldt et al.*, 2005]. Oxygen concentrations were determined using amperometric Clark-type oxygen sensors 12 h after core recovery to allow for temperature equilibration. For Site 15, nitrate measurements were performed photometrically on board using a continuous flow injection system based on the sulfanile-α-naphthylamide method [*Mewes et al.*, 2014]. Nitrate samples for Site 54 and Site 55 were diluted 1:2 with demineralized water and stored frozen until analysis in the home laboratory using the same method. Dissolved reduced manganese (Mn^{2+}) was measured with inductively coupled plasma optical emission spectrometry after a 1:10 dilution and acidification with HNO_3. Total organic carbon (TOC) contents were determined by combustion analysis with a CS 2000 carbon-sulfur determinator. The burial velocity of solids was calculated using the decay of beryllium-10 with depth and taking sediment compaction into account. Further details are available in *Mewes et al.* [2014].

2.2. Model Setup and Reaction Network

Geochemical interactions were simulated using a one-dimensional reaction-transport model [*Mewes et al.*, 2016] which discretizes the advection-diffusion-reaction equation [e.g., *Berner*, 1980; *Boudreau*, 1997; *Mogollón et al.*, 2012]. The model consists of seven reactions (Table 1) and includes organic matter as the sole solid species (*G*, Tables 1 and 2), and four dissolved species (*C*, Tables 1 and 2). It includes the effects of biologically induced mixing via diffusive (bioturbation) and nonlocal (bioirrigation) transport terms [*Mewes et al.*, 2016]. For further details see supporting information.

The primary redox reactions involving organic matter degradation (R_1–R_3) were simulated using a reactive continuum of organic matter pools described through a Gamma distribution [*Boudreau and Ruddick*, 1991]. Aerobic respiration (R_1) was considered as the most favorable pathway of organic matter consumption [*Froelich and et al.*, 1979]. The inhibition factor for denitrification (h_1) was set to 0.1 μ*M* (for a sensitivity analysis

Table 1. Electron-Equivalent Chemical Reactions and Associated Rate Expressions Used in the Numerical Model[a]

Name	ID	Reaction	Rate Expression	Rate Unit
Organic matter degradation	R_1	$\frac{1}{4}(\mathbf{CH_2O})(\mathbf{NH_3})_\mathbf{b} + \frac{1}{4}\mathbf{O_2} + \frac{b}{4}H^+$	$\frac{\sigma G_{TOC}^{1+1/\sigma}}{a G_{TOC,0}^{1/\sigma}} \frac{C_{O_2}}{C_{O_2}+h_1}$	$\frac{mmolC}{l(drysediment)y}$
degradation		$\rightarrow \frac{1}{4}\mathbf{CO_2} + \frac{b}{4}\mathbf{NH_4^+} + \frac{1}{4}H_2O$		
Heterotrophic denitrification	R_2	$\frac{1}{4}(\mathbf{CH_2O})(\mathbf{NH_3})_\mathbf{b} + \frac{1}{5}\mathbf{NO_3^-} + (\frac{1}{5}+\frac{b}{4})H^+$	$\frac{\sigma G_{TOC}^{1+1/\sigma}}{a G_{TOC,0}^{1/\sigma}} \gamma \frac{C_{NO_3^-}}{C_{NO_3^-}+h_2}$	$\frac{mmolC}{l(drysediment)y}$
		$\rightarrow \frac{1}{10}N_2 + \frac{1}{4}CO_2 + \frac{b}{4}\mathbf{NH_4^+} + \frac{7}{20}H_2O$		
Manganese oxide reduction	R_3	$\frac{1}{4}(\mathbf{CH_2O})(\mathbf{NH_3})_\mathbf{b} + \frac{1}{2}MnO_2 + (1+\frac{b}{4})H^+$	$\frac{\sigma G_{TOC}^{1+1/\sigma}}{a G_{TOC,0}^{1/\sigma}} \gamma \frac{h_2}{C_{NO_3^-}+h_2}$	$\frac{mmolC}{l(drysediment)y}$
		$\rightarrow \frac{1}{2}\mathbf{Mn^{2+}} + \frac{1}{4}CO_2 + \frac{b}{4}\mathbf{NH_4^+} + \frac{3}{4}H_2O$		
Manganese oxidation	R_4	$\frac{1}{2}\mathbf{Mn^{2+}} + \frac{1}{4}\mathbf{O_2} + \frac{1}{2}H_2O$	$k_4 C_{O_2} C_{Mn^{2+}}$	$\frac{\mu M\, O_2}{y}$
		$\rightarrow \frac{1}{2}MnO_2 + H^+$		
Nitrification	R_5	$\frac{1}{4}\mathbf{O_2} + \frac{1}{8}\mathbf{NH_4^+}$	$k_5 C_{O_2} C_{NH_4^+}$	$\frac{\mu M\, N}{y}$
		$\rightarrow \frac{1}{8}\mathbf{NO_3^-} + \frac{1}{4}H^+ + \frac{1}{8}H_2O$		
Mn^{2+}-mediated	R_6	$\frac{1}{5}\mathbf{NO_3^-} + \frac{1}{2}\mathbf{Mn^{2+}} + \frac{2}{5}H_2O$	$k_6 C_{NO_3^-} C_{Mn^{2+}}$	$\frac{\mu M\, N}{y}$
denitrification		$\rightarrow \frac{1}{2}MnO_2 + \frac{4}{5}H^+ + \frac{1}{10}N_2$		
Mn-anammox	R_7	$\frac{1}{2}MnO_2 + \frac{1}{3}\mathbf{NH_4^+} + \frac{2}{3}H^+$	$k_7 C_{NH_4^+} \gamma \epsilon$	$\frac{\mu M\, N}{y}$
		$\rightarrow \frac{1}{2}\mathbf{Mn^{2+}} + \frac{1}{6}N_2 + H_2O$		

[a] b was assumed to follow the Redfield ratio stoichiometry of organic-bound nitrogen to organic carbon of 16:106. a and σ are parameters that dictate the degradation of organic matter (see text). Values in bold represent the explicitly modeled species. $\gamma = h_1/(h_1 + C_{O_2})$, $\epsilon = \frac{\exp\left(\frac{t_1 - C_{NO_3^-}}{t_2}\right)}{1+\exp\left(\frac{t_1 - C_{NO_3^-}}{t_2}\right)}$.

of this parameter see supporting information). Denitrification (R_2) was assumed to inhibit manganese oxide reduction (R_3). Due to the high concentration of reactive manganese oxide in the sediment, a high inhibition factor for manganese oxide reduction (h_2=30 μ*M*, Table 3) was implemented [*Boudreau*, 1996]. Reactions R_4 and R_5, representing aerobic manganese oxidation and nitrification, respectively, were represented through bimolecular kinetics. R_6, which represents the Mn^{2+}-coupled denitrification, further includes an inhibition term (γ, Table 1) when oxygen is present. This denitrification pathway parallels that considered for reduced iron [e.g., *Weber et al.*, 2006]. *Luther et al.* [1997], after observations at three sites off the coast of

Table 2. Species, Boundary Conditions, and Parameter Values Used in the Reaction-Transport Model[a]

			BC SWI Value			
Name	Symbol	BC SWI Type (Unit)	St. 54	St. 55	St. 15	Reaction Terms ($\sum R_i$)
		Species and Boundary Conditions				
Total organic carbon	CH_2O	Flux (mol m^{-2} yr^{-1})	0.046	0.21	0.35	$-R_1 - R_2 - R_3$
Oxygen	O_2	Concentration (μ*M*)	145.7	155.0	152.6	$-\eta R_1 - R_4 - 2R_5$
Ammonium	NH_4^+	Concentration (μ*M*)	0.1	0.1	0.1	$\frac{16}{106}\eta(R_1+R_2+R_3) - R_5 - R_7$
Nitrate	NO_3^-	Concentration (μ*M*)	44	47	43	$-\frac{4}{5}\eta R_2 + R_5 - R_6$
Dissolved reduced manganese	Mn^{2+}	Concentration (μ*M*)	0.0	0.0	0.0	$2\eta R_3 - 2R_4 - \frac{5}{2}R_6 + \frac{3}{2}R_7$

[a] BC = boundary condition and SWI = sediment-water interface. Total organic carbon is the only solid species present in the model. All other species are dissolved. $\eta = \frac{1-\theta}{\theta}\frac{\rho_d}{m_C}\frac{1}{100\%}$, ρ_d is the dry bulk density (2.6 g cm^{-3}), and m_C = molar weight of carbon (12 g mol^{-1}).

Table 3. Species, Boundary Conditions, and Parameter Values Used in the Reaction-Transport Model[a]

Name	Symbol	Unit	54	55	15
	Fitted Parameters				
Solid burial velocity at compaction	w_∞	cm ky^{-1}	0.333	0.536	0.527
TOC degradation time constant	a	year	11.0	1.0	0.7
TOC degradation apparent order	σ	-	0.07	0.1	0.13
R_4 rate constant	k_4	μM^{-1} y^{-1}	0.11	0.11	0.11
Bioturbation coefficient	$D_{b,0}$	cm yr^{-1}	15.0	2.6	0.7
Biomixing half depth	z_{mix}	cm	5.0	5.0	5.0
Biomixing attenuation	z_{att}	cm	5.0	5.0	5.0
R_1 O_2 inhibition concentration	h_1	μM	0.01	0.01	0.01
R_2 NO_3^- inhibition concentration	h_2	μM	30.0	30.0	30.0
Bioirrigation coefficient	α_0	y^{-1}	1.65	5.0	2.85
R_5 rate constant	k_5	μM^{-1} yr^{-1}	0.01	0.0017	0.0035
R_6 rate constant	k_6	μM^{-1} yr^{-1}	3.0E-6	1.8E-6	5.0E-6
R_7 rate constant	k_7	y^{-1}	0.02	0.05	0.0035
R_7 NO_3^- inhibition concentration	ι_1	μM	11.0	51.5	9.5
R_7 reaction rate concentration	ι_2	μM	3.0	0.7	7.9

[a]BC = boundary condition and SWI = sediment-water interface. Total organic carbon is the only solid species present in the model. All other species are dissolved. $\eta = \frac{1-\theta}{\theta}\frac{\rho_d}{m_C}\frac{1}{100\%}$, ρ_d is the dry bulk density (2.6 g cm^{-3}), and m_C = molar weight of carbon (12 g mol^{-1}).

Nova Scotia, described two pathways by which NH_4^+ could reduce manganese oxides, one leading to NO_3^- formation and one leading to dinitrogen (N_2) directly. Similar reactions have been proposed with iron oxides through an initial conversion of NH_4^+ to nitrite (NO_2^-) [*Clément et al.*, 2005; *Yang et al.*, 2012]. Here we consider a similar pathway for manganese oxides:

$$\frac{1}{2}MnO_2 + \mathbf{\frac{1}{6}NH_4^+} + \frac{2}{3}H^+ \rightarrow \mathbf{\frac{1}{2}Mn^{2+}} + \frac{1}{6}NO_2^- + \frac{2}{3}H_2O. \quad (1)$$

NO_2^- can then oxidize NH_4^+ via the traditional anammox reaction [*Kuypers et al.*, 2003]:

$$\mathbf{\frac{1}{6}NH_4^+} + \frac{1}{6}NO_2^- \rightarrow \frac{1}{6}N_2 + \frac{1}{3}H_2O. \quad (2)$$

R_7 (Table 1) represents the net process for (1) and (2). We assume that it can be mathematically quantified as a one-step reaction, which precludes that (1) is rate limiting and that anammox (2) occurs as soon as any NO_2^- is generated from (1). R_7 was described through a first-order degradation with respect to the ammonium concentration with an inhibition term under high nitrate concentrations. This inhibition was implemented through a sigmoidal function (ϵ, Table 1), which follows previous findings that high nitrate concentrations may impede Mn-anammox [*Javanaud et al.*, 2011]. The oxidation of Mn^{2+} in suboxic water columns [*Trouwborst et al.*, 2006; *Oldham et al.*, 2015] and a single electron reduction of manganese oxide at the interface of oxic-anoxic sediments [*Madison et al.*, 2013] may lead to an intermediate Mn^{3+} species. Mn^{3+} requires stabilizing ligands (most which are organic) and thus may not be dominant in these sediments. Nevertheless, we cannot exclude the presence of Mn^{3+}, but it could undergo similar coupled Mn-N reaction pathways with altered stoichiometries to those presented here. More work is thus required to explore the possibility of Mn^{3+} and its interactions in these settings. The model simulations assume that the geochemical profiles, including all implicit reactive intermediates, are near steady state.

3. Results and Discussion

3.1. Description of Geochemical Profiles

At all stations, organic matter (total organic carbon, TOC) and oxygen (O_2) profiles decrease exponentially with depth, with the greatest loss (>50% of the concentrations at the sediment surface) occurring within the

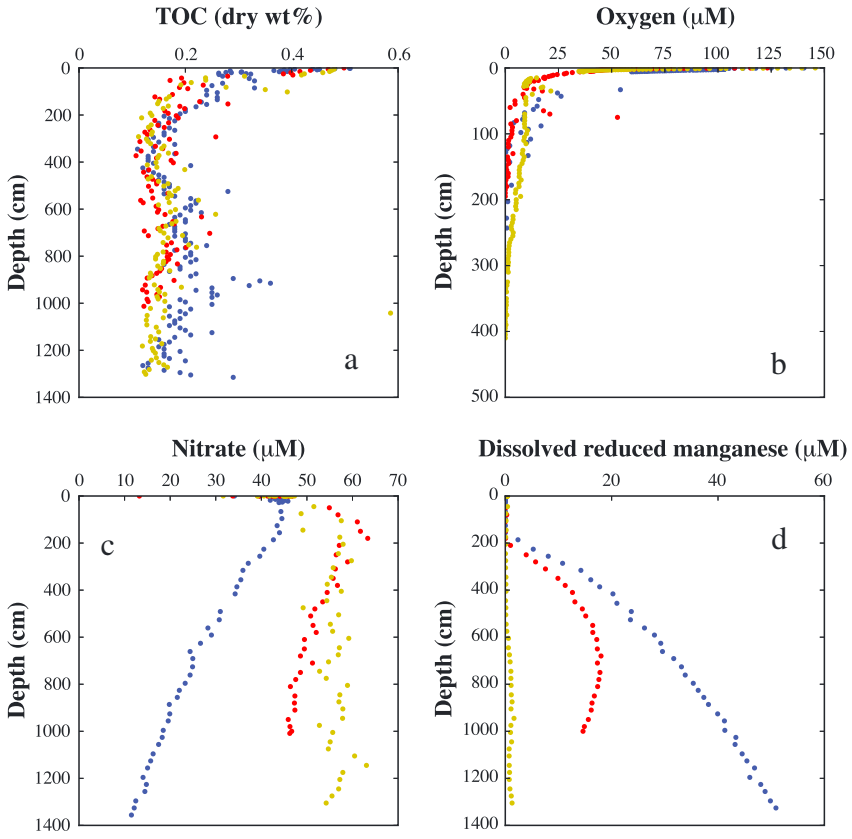

Figure 2. Measured data [*Mewes et al.*, 2014] for (a) total organic carbon (TOC, (b) oxygen, (c) nitrate, and (d) dissolved reduced manganese for Station 54 (yellow), Station 55 (red), and Station 15 (blue). Note the different depth scale for Figure 2b.

uppermost 20 cm of the sediment [*Mewes et al.*, 2014]. While TOC profiles at all stations level off at approximately 0.2 wt % (Figure 2), O_2 becomes exhausted at 350 cm depth, 200 cm depth, and 150 cm depth for Station 54, Station 55, and Station 15, respectively (Figure 2). Similar OPDs have been increasingly encountered in the deep sea, e.g., at the edge of the South Pacific Gyre [*D'Hondt et al.*, 2009] and in the mid-Atlantic regions [*Ziebis et al.*, 2012]. Sedimentation rates (burial rates at compaction) at Station 15 and Station 55 are relatively similar at 0.527 cm ky^{-1} and 0.533 cm ky^{-1}, respectively, but markedly higher than the 0.333 cm ky^{-1} calculated for Station 54 [*Mewes et al.*, 2014]. The deposition of sedimentary material in the CCFZ depends on the intensity of the bottom water currents. These currents are highly localized and generally follow the topography of the area, which contains many horst and graben (large, oriented block fault) structures and seamounts [*Rühlemann et al.*, 2011]. These currents are also subject to seasonal variations which may affect depositional patterns even at the subkilometer scale [*Halbach et al.*, 1988; *Mewes et al.*, 2014].

NO_3^- and Mn^{2+} profiles show pronounced variations at the three study sites. Station 54 is characterized by low Mn^{2+} concentrations (< 5 μ*M*) and a plateau in the NO_3^- profile at depth. Station 55 is characterized by a Mn^{2+} profile which increases with depth until its zenith of 18 μ*M* at 650 cm depth and a subsequent concentration decrease with depth, and a NO_3^- profile which exhibits a slight decrease in concentration with depth. Station 15 is characterized by a concave up Mn^{2+} profile and a concomitant NO_3^- profile that decreases with depth. Neither free iron nor sulfide was detected at any of the measured stations. MnO_2 values typically exceed 0.1 dry wt %, indicating a system relatively rich in manganese oxides [*Mewes et al.*, 2014]. Contrary to the classical redox sequence in which NO_3^- reduction precedes manganese oxide reduction [*Froelich and et al.*, 1979], Mn^{2+} is actively produced in the presence of high (>40 μ*M*) NO_3^- concentrations at the three study sites. For example, at Station 55 an evident Mn^{2+} peak occurs at a depth where the NO_3^- concentration is roughly 50 μ*M*. NO_3^- concentrations decrease with increasing Mn^{2+} concentrations, which further supports a suboxic coupling between the nitrogen and manganese cycles [*Luther et al.*, 1997; *Hulth et al.*, 1999; *Aller et al.*, 1998; *Anschutz et al.*, 2000, 2005; *Bartlett et al.*, 2008; *Hulth et al.*, 2005; *Mortimer et al.*, 2004]. We hypothesize that this

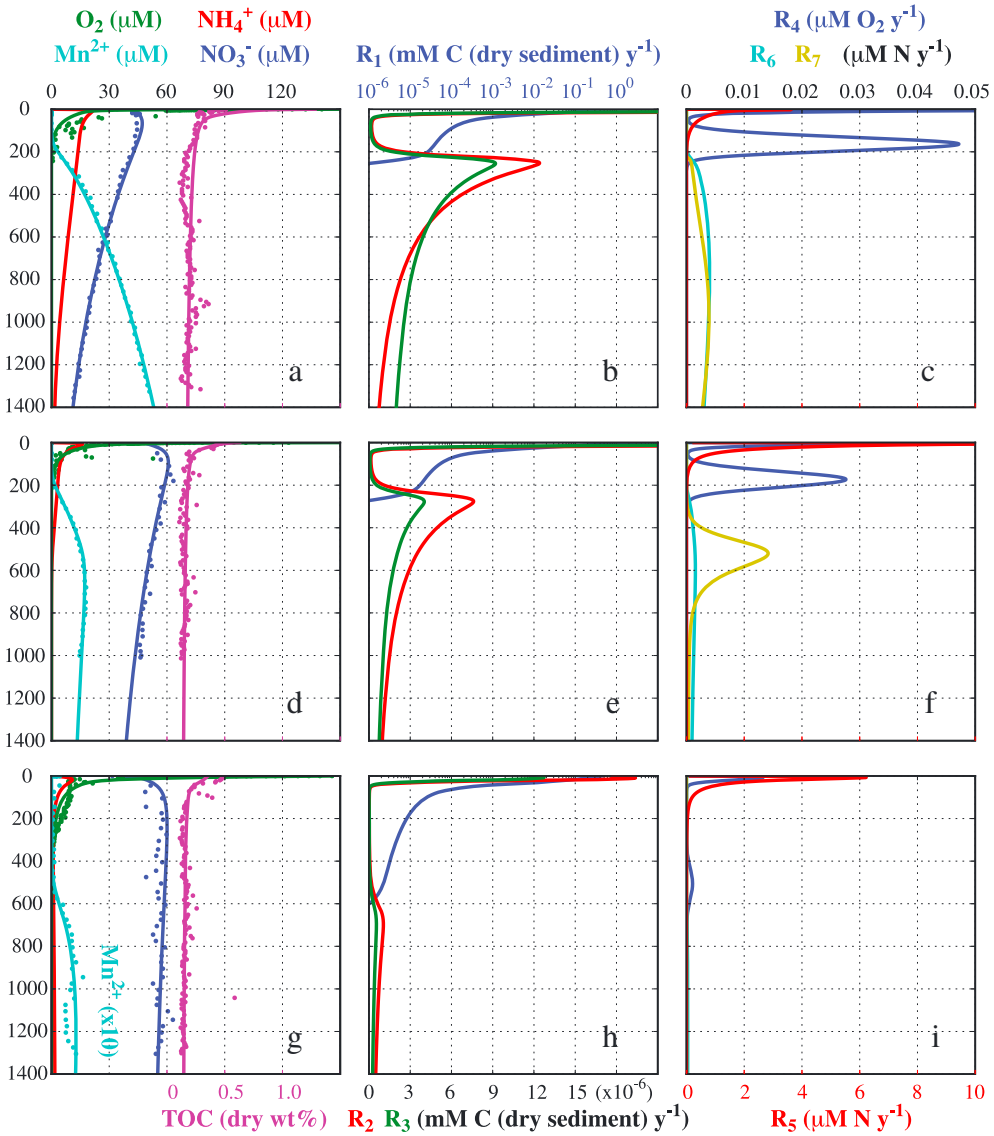

Figure 3. Model results for (a–c) Station 54, (d–f) Station 55, and (g–i) Station 15. Measured and modeled profiles (Figures 3a, 3d, and 3g) are compared when available. Primary redox reactions rates involving the heterotrophic degradation of organic matter (Figures 3b, 3e, and 3h) and the autotrophic secondary redox reactions rates (Figures 3c, 3f, and 3i) represent the rates listed in Table 1. Note that Mn^{2+} has a different scale in Figure 3g.

coupling comes about due to the interaction of reduced nitrogen species with oxidized manganese species and vice versa, leading to additional pathways for dinitrogen formation.

3.2. Quantifying Mn-N Coupling

Organic carbon fluxes of 0.046 mol m^{-2} yr^{-1} (Station 54), 0.21 mol m^{-2} yr^{-1} (Station 55), and 0.35 mol m^{-2} yr^{-1} (Station 15) obtained from the model simulations (Figure 3, see Text S5 in the supporting information) compare well with the previously estimated flux in nearby regions of 0.05–0.3 mol m^{-2} yr^{-1} [*Murray and Kuivila*, 1990]. The model suggests that organic matter degradation is low below the oxic zone, with rates at the OPD less than 1% those at deposition (Figure 3). The bulk of the organic matter degradation takes place within the oxic zone (depth-integrated R_1 > 99% of total, Figure 3). Here most of the ammonium liberated from the degradation of organic matter becomes nitrified, which leads to the increasing-with-depth NO_3^- profiles within the top meter of the sediment. The low sedimentation rates limit reactive organic carbon from reaching the suboxic zone, and thus, organic carbon becomes insufficient to completely reduce NO_3^- and liberate Mn^{2+} to above 5 μ*M* concentrations, as is the case for Station 54. The age of the sediment at the

contemporary OPD reaches the 10^6 y range, and thus, the organic carbon located below the OPD is highly refractory, with apparent first-order degradation constants in the 10^{-8} yr^{-1} range.

Due to the low and refractory organic carbon content, the microbe-mediated autotrophic secondary reactions dominate the geochemistry below the OPD. Nevertheless, each station undergoes these geochemical transformations at vastly different rates. At Station 54, nitrification exceeds all other stations (Figure 3), and thus, the depletion of ammonium within the oxic zone is also, comparatively, the largest. As NO_3^- may inhibit Mn-anammox [*Javanaud et al.*, 2011], we postulate that the refractive organic matter available below the OPD is unable to consume NO_3^- to levels which would permit a favorable R_7 reaction. Conversely, this highly refractive organic matter is the main reductant available below the oxic zone, and thus, NO_3^- and manganese oxide reduction rates are considerably lower (depth-integrated rates of 1.62 10^{-5} mol C m^{-2} yr^{-1} and 9.15 10^{-6} mol C m^{-2} yr^{-1}, respectively) in comparison to the depth-integrated rates of organic carbon respiration (4.58 10^{-2} mol C m^{-2} yr^{-1}).

Nevertheless, at Station 55 and Station 15, higher sedimentation rates and higher organic matter fluxes allow for sufficiently high aerobic and suboxic organic matter degradation rates which generate enough ammonium to overcome nitrification and diffuse below the Ocean Drilling Program (ODP) to deliver additional reducing potential for manganese oxide reduction (via R_7). While ammonium was not measured at these sites, ammonium measurements at nearby sites (Figure 1) from international deep-sea drilling projects agree with the general observations of this study. For instance, ODP site 854B [*Mayer et al.*, 1992] shows no detectable ammonium below 3 m sediment depth, while at integrated ODP site 1218A [*Lyle et al.*, 2002] ammonium hovers around 11 μM within the uppermost 30 m of the sediment. These low ammonium concentrations may not be favorable to trigger the extended anammox reaction involving nitrate as an oxidizer as opposed to nitrite [*Kartal et al.*, 2007]; however, they may be sufficient to trigger manganese oxide reduction in environments where the concentrations of manganese oxides greatly exceed those of nitrate [*Javanaud et al.*, 2011].

Simulation results at Station 55 and Station 15 (Figures 4a–4c) reveal that Mn-anammox potentially represents an important pathway for N_2 export, accounting for 28% and 27% of N_2 formation, respectively. These values are marginally lower than anammox percentages in anoxic environments using a regression according to the C-H-O stoichiometry of the organic matter [*Babbin et al.*, 2014] but fall within published anammox percentage ranges [*Devol*, 2015]. The slightly lower anammox contribution here could be due to ammonium transport limitation from the oxic zone to the suboxic zone, which arises from both the expanded redox zonation leading to larger diffusive lengths, and the lower ammonium release rates from the sluggish organic carbon degradation. Manganese-nitrogen cycle coupling is further hypothesized to occur with the Mn^{2+} partially reducing NO_3^- to N_2, a process which has been previously speculated but not demonstrated [*Luther et al.*, 1997; *Bartlett et al.*, 2008]. This reaction provides an additional suboxic export of N_2, representing roughly 24%, and 37% of the total N_2 formation for Station 55 and Station 15, respectively (Figures 4a–4c). These rates thus represent a significant contribution to dinitrogen formation. In comparison, N_2 production from the organic matter-coupled reduction of nitrate is mainly limited to the bioturbated portion of the sediment where the highest rates of organic matter degradation contribute toward the highest rates of denitrification (Figure 3). Although difficult to assess due to biogenically induced mixing, nitrification and denitrification processes in the upper centimeters of the sediment may impose an important control on nitrogen export.

Previous Mn-anammox studies in anoxic sediments have yielded inconclusive results about its influence on the N and Mn cycles. Some incubation experiments [e.g., *Anschutz et al.*, 2005; *Bartlett et al.*, 2008; *Hulth et al.*, 1999, 2005; *Lin and Taillefert*, 2014] and geochemical profile evaluations [e.g., *Luther et al.*, 1997; *Aller et al.*, 1998; *Anschutz et al.*, 2000; *Mortimer et al.*, 2004] provide support for this process; whereas other incubation experiments [e. g., *Thamdrup and Dalsgaard*, 2000; *Engström et al.*, 2005] found this process to be insignificant. It is important to note, however, that these studies were mainly performed in (or with) organic carbon-rich anoxic sediments. Thus, heterotrophic manganese oxide reduction, which has even been postulated to inhibit Mn-anammox [*Bartlett et al.*, 2008], would overprint the reduction of manganese oxides in the presence of NH_4^+. Furthermore, discerning the pathway for NH_4^+ consumption in systems with abundant manganese and iron oxides, as well as nitrite, may prove challenging.

Unlike the nitrogen cycle, which is governed by processes taking place in both the oxic and suboxic zones, the Mn cycle takes place mainly within the suboxic zone. Oxygenotrophic Mn^{2+} oxidation (R_4, Table 1) is evident but occurs at rates which are substantially lower with respect to the other depth-integrated Mn-cycle reaction rates. At Station 55 and Station 15, ammonium-triggered Mn^{2+} release represents a substantial portion

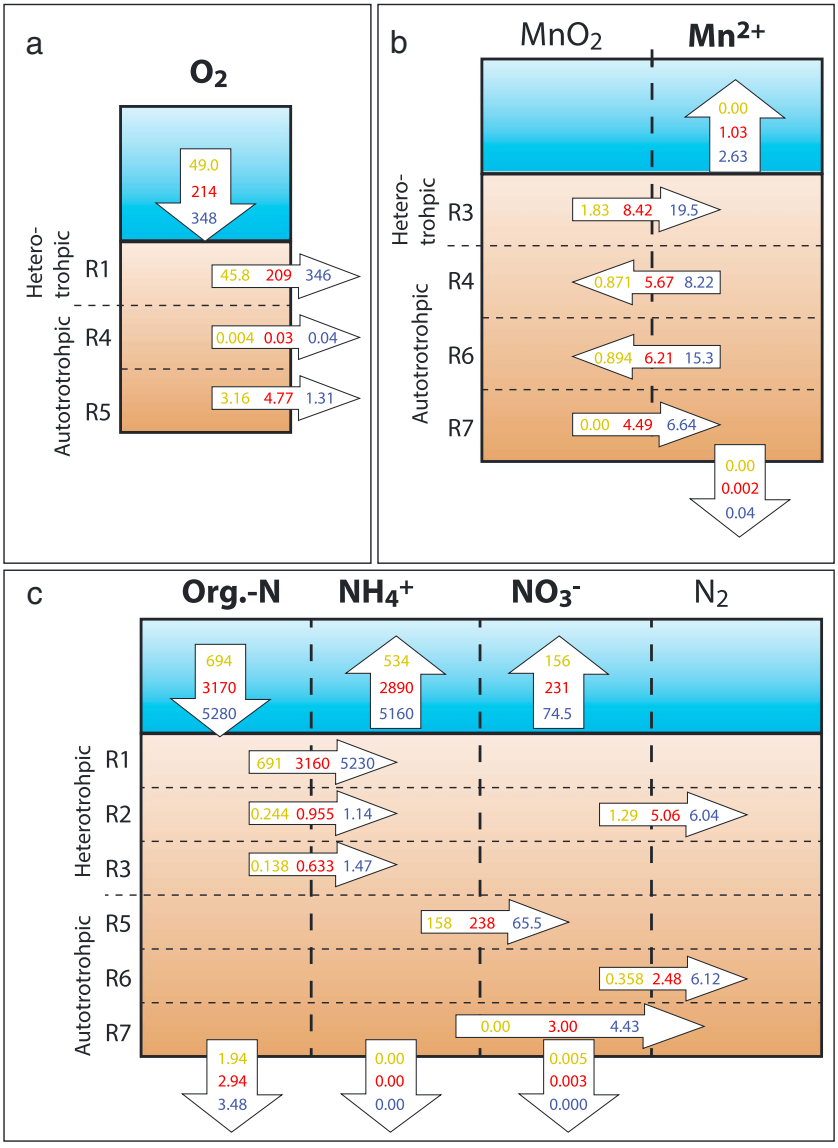

Figure 4. Geochemical cycling for oxygen ((a) in 10^{-3} mol O_2 m^{-2} yr^{-1}), manganese ((b) in 10^{-5} mol Mn m^{-2} yr^{-1}), and nitrogen ((c) in 10^{-5} mol N m^{-2} yr^{-1}) for Station 54 (yellow), Station 55 (red), and Station 15 (blue). Vertical arrows represent fluxes in and out of the sediment (top) or into/out of the lower model boundary (50 m). Horizontal arrows represent reaction rates according to Table 1. Species in bold are explicitly included in the model.

(30% and 25%, respectively) of Mn^{2+} liberation. Continuous diffusion of NH_4^+ into the suboxic zone can thus lead to the buildup of Mn^{2+} in the sediment which may play a factor in Mn-nodule growth during periods of more reducing conditions in the sediment.

4. Conclusion

In this study, field data from the CCFZ providing evidence of Mn-mediated nitrogen cycling in carbon-starved, suboxic sediments, were quantified using a reaction-transport model with reactions involving the Mn and N cycles. Geochemical process in other organic carbon-starved sediments such as the Pacific Gyres [*D'Hondt et al.*, 2009] and the South East Atlantic [*Gingele and Kasten*, 1994], where the distribution of microbial activities has been found to be relatively diverse [*D'Hondt et al.*, 2004], may represent important yet largely unexplored fractions of subsurface geochemistry. In these sediments, the expanded redox zonation can thus help in constraining the various interactions between oxidized and reduced species, and especially the interactions

between the N, Mn, and even the Fe cycles. In the CCFZ, results indicate that Mn-mediated pathways can account for more than half of reactive nitrogen removal. This finding stresses the need to further investigate the influence of manganese (and iron) cycles on global N_2 formation.

Acknowledgments
This research was funded by the Bundesministerium für Bildung und Forschung (BMBF; grant 03G0205C) and by the European Commission through Marie Skłodowska Curie Individual Fellow ship grant 661163 to José M. Mogollón. We acknowledge further financial support from the Helmholtz Association (Alfred Wegener Institute Helmholtz Centre for Polar and Marine Research, Bremerhaven). An executable version of the model can be made available by contacting the corresponding author.

References

Aller, R. C., P. O. Hall, P. D. Rude, and J. Aller (1998), Biogeochemical heterogeneity and suboxic diagenesis in hemipelagic sediments of the Panama Basin, *Deep Sea Res., Part I*, *45*(1), 133–165, doi:10.1016/S0967-0637(97)00049-6.

Anschutz, P., B. Sundby, L. Lefran cois, G. W. Luther, and A. Mucci (2000), Interactions between metal oxides and species of nitrogen and iodine in bioturbated marine sediments, *Geochim. Cosmochim. Acta*, *64*(16), 2751–2763, doi:10.1016/S0016-7037(00)00400-2.

Anschutz, P., K. Dedieu, F. Desmazes, and G. Chaillou (2005), Speciation, oxidation state, and reactivity of particulate manganese in marine sediments, *Chem. Geol.*, *218*(3–4), 265–279, doi:10.1016/j.chemgeo.2005.01.008.

Babbin, A. R., R. G. Keil, A. H. Devol, and B. B. Ward (2014), Organic matter stoichiometry, flux, and oxygen control nitrogen loss in the ocean, *Science*, *344*(6182), 406–408, doi:10.1126/science.1248364.

Bartlett, R., R. J. Mortimer, and K. Morris (2008), Anoxic nitrification: Evidence from Humber Estuary sediments (UK), *Chem. Geol.*, *250*(1–4), 29–39, doi:10.1016/j.chemgeo.2008.02.001.

Berner, R. (1980), *Early Diagenesis: A Theoretical Apporach*, Princeton Univ. Press, New York.

Boudreau, B. (1997), Diagenetic models and their implementations.

Boudreau, B., and B. Ruddick (1991), On a reactive continuum representation of organic-matter diagenesis, *Am. J. Sci.*, *291*(5), 507–538.

Boudreau, B. P. (1996), A method-of-lines code for carbon and nutrient diagenesis in aquatic sediments, *Comput. Geosci.*, *22*(5), 479–496, doi:10.1016/0098-3004(95)00115-8.

Clément, J.-C., J. Shrestha, J. G. Ehrenfeld, and P. R. Jaffé (2005), Ammonium oxidation coupled to dissimilatory reduction of iron under anaerobic conditions in wetland soils, *Soil Biol. Biochem.*, *37*(12), 2323–2328, doi:10.1016/j.soilbio.2005.03.027.

Devol, A. H. (2015), Denitrification, anammox, and n_2 production in marine sediments, *Annu. Rev. Mar. Sci.*, *7*(1), 403–423, doi:10.1146/annurev-marine-010213-135040.

D'Hondt, S. et al. (2004), Distributions of microbial activities in deep subseafloor sediments, *Science*, *306*(5705), 2216–2221, doi:10.1126/science.1101155.

D'Hondt, S., et al. (2009), Subseafloor sedimentary life in the South Pacific gyre, *Proc. Natl. Acad. Sci.*, *106*(28), 11,651–11,656, doi:10.1073/pnas.0811793106.

Dunne, J. P., J. L. Sarmiento, and A. Gnanadesikan (2007), A synthesis of global particle export from the surface ocean and cycling through the ocean interior and on the seafloor, *Global Biogeochem. Cycles*, *21*(4), GB4006, doi:10.1029/2006GB002907.

Engström, P., T. Dalsgaard, S. Hulth, and R. C. Aller (2005), Anaerobic ammonium oxidation by nitrite (anammox): Implications for N_2 production in coastal marine sediments, *Geochim. Cosmochim. Acta*, *69*(8), 2057–2065, doi:10.1016/j.gca.2004.09.032.

Fischer, M., I. Zinovik, and D. Poulikakos (2009), Diffusion and reaction controlled dissolution of oxygen microbubbles in blood, *Int. J. Heat Mass Transfer*, *52*(21–22), 5013–5019, doi:10.1016/j.ijheatmasstransfer.2009.05.013.

Froelich, P., et al. (1979), Early oxidation of organic matter in pelagic sediments of the eastern equatorial Atlantic: Suboxic diagenesis, *Geochim. Cosmochim. Acta*, *43*(7), 1075–1090, doi:10.1016/0016-7037(79)90095-4.

Gingele, F. X., and S. Kasten (1994), Solid-phase manganese in Southeast Atlantic sediments: Implications for the paleoenvironment, *Mar. Geol.*, *121*(3–4), 317–332, doi:10.1016/0025-3227(94)90037-X.

Halbach, P., G. Friedrich, and U. Stackelber (1988), *The Manganese Nodule Belt of the Pacific Ocean*, 254, Enke, Stuggart.

Hulth, S., R. C. Aller, and F. Gilbert (1999), Coupled anoxic nitrification/manganese reduction in marine sediments, *Geochim. Cosmochim. Acta*, *63*(1), 49–66, doi:10.1016/S0016-7037(98)00285-3.

Hulth, S., R. C. Aller, D. E. Canfield, T. Dalsgaard, P. Engström, F. Gilbert, K. Sundbäck, and B. Thamdrup (2005), Nitrogen removal in marine environments: Recent findings and future research challenges, *Mar. Chem.*, *94*(1–4), 125–145, doi:10.1016/j.marchem.2004.07.013.

Javanaud, C., V. Michotey, S. Guasco, N. Garcia, P. Anschutz, M. Canton, and P. Bonin (2011), Anaerobic ammonium oxidation mediated by Mn-oxides: From sediment to strain level, *Res. Microbiol.*, *162*(9), 848–857, doi:10.1016/j.resmic.2011.01.011.

Kartal, B., M. M. M. Kuypers, G. Lavik, J. Schalk, H. J. M. Op den Camp, M. S. M. Jetten, and M. Strous (2007), Anammox bacteria disguised as denitrifiers: Nitrate reduction to dinitrogen gas via nitrite and ammonium, *Environ. Microbiol.*, *9*(3), 635–642, doi:10.1111/j.1462-2920.2006.01183.x.

Kuypers, M. M. M., A. O. Sliekers, G. Lavik, M. Schmid, B. B. Jørgensen, J. G. Kuenen, J. S. Sinninghe Damsté, M. Strous, and M. S. M. Jetten (2003), Anaerobic ammonium oxidation by anammox bacteria in the Black Sea, *Nature*, *422*(6932), 608–611.

Lin, H., and M. Taillefert (2014), Key geochemical factors regulating Mn(IV)-catalyzed anaerobic nitrification in coastal marine sediments, *Geochim. Cosmochim. Acta*, *133*, 17–33, doi:10.1016/j.gca.2014.01.025.

Luther, G. W., B. Sundby, B. L. Lewis, P. J. Brendel, and N. Silverberg (1997), Interactions of manganese with the nitrogen cycle: Alternative pathways to dinitrogen, *Geochim. Cosmochim. Acta*, *61*(19), 4043–4052, doi:10.1016/S0016-7037(97)00239-1.

Lyle, M., et al. (2002), Site 1218, *Proceedings of the Ocean Drilling Program, Initial Reports*, *199*, 1–126.

Madison, A. S., B. M. Tebo, A. Mucci, B. Sundby, and G. W. Luther (2013), Abundant porewater Mn(III) is a major component of the sedimentary redox system, *Science*, *341*(6148), 875–878, doi:10.1126/science.1241396.

Mayer, L., et al. (1992), Site 854, *Proceedings of the Ocean Drilling Program, Initial Reports*, *138*, 1063–1092.

Mewes, K., J. Mogollón, A. Picard, C. Rühlemann, T. Kuhn, K. Nöthen, and S. Kasten (2014), Impact of depositional and biogeochemical processes on small scale variations in nodule abundance in the Clarion-Clipperton Fracture Zone, *Deep Sea Res., Part I*, *91*(0), 125–141, doi:10.1016/j.dsr.2014.06.001.

Mewes, K., J. Mogollón, A. Picard, C. Rühlemann, A. Eisenhauer, T. Kuhn, W. Ziebis, and S. Kasten (2016), Diffusive transfer of oxygen from seamount basaltic crust into overlying sediments: An example from the clarion–clipperton fracture zone, *Earth Planet. Sci. Lett.*, *433*, 215–225, doi:10.1016/j.epsl.2015.10.028.

Mogollón, J. M., A. W. Dale, H. Fossing, and P. Regnier (2012), Timescales for the development of methanogenesis and free gas layers in recently-deposited sediments of Arkona Basin (Baltic Sea), *Biogeosciences*, *9*, 1915–1933, doi:10.5194/bg-9-1915-2012.

Mortimer, R. J. G., S. J. Harris, M. D. Krom, T. E. Freitag, J. I. Prosser, J. Barnes, P. Anschutz, P. J. Hayes, and I. M. Davies (2004), Anoxic nitrification in marine sediments, *Mar. Ecol. Prog. Ser.*, *276*, 37–52.

Murray, J. W., and K. M. Kuivila (1990), Organic matter diagenesis in the northeast Pacific: Transition from aerobic red clay to suboxic hemipelagic sediments, *Deep Sea Res., Part A*, *37*(1), 59–80, doi:10.1016/0198-0149(90)90029-U.

Oldham, V. E., S. M. Owings, M. R. Jones, B. M. Tebo, and G. W. L. III (2015), Evidence for the presence of strong mn(iii)-binding ligands in the water column of the Chesapeake Bay, *Mar. Chem.*, *171*, 58–66, doi:10.1016/j.marchem.2015.02.008.

Røy, H., J. Kallmeyer, R. R. Adhikari, R. Pockalny, B. B. Jørgensen, and S. D'Hondt (2012), Aerobic microbial respiration in 86-million-year-old deep-sea red clay, *Science*, *336*(6083), 922–925, doi:10.1126/science.1219424.

Rühlemann, C., T. Kuhn, M. Wiedicke, S. Kasten, K. Mewes, and A. Picard (2011), Current status of manganese nodule exploration in the german license area, in *Proceedings of the 9th (2011) ISOPE Ocean Mining Symposium*, pp. 168–173, International Society of Offshore and Polar Engineers (ISOPE), Maui.

Seeberg-Elverfeldt, J., M. Schlüter, T. Feseker, and M. Kölling (2005), Rhizon sampling of pore waters near the sediment/water interface of aquatic systems, *Limnol. Oceanogr. Methods*, *3*, 361–371, doi:10.4319/lom.2005.3.361.

Thamdrup, B., and T. Dalsgaard (2000), The fate of ammonium in anoxic manganese oxide-rich marine sediment, *Geochim. Cosmochim. Acta*, *64*(24), 4157–4164, doi:10.1016/S0016-7037(00)00496-8.

Trouwborst, R. E., B. G. Clement, B. M. Tebo, B. T. Glazer, and G. W. Luther (2006), Soluble Mn(III) in suboxic zones, *Science*, *313*(5795), 1955–1957, doi:10.1126/science.1132876.

Weber, K. A., L. A. Achenbach, and J. D. Coates (2006), Microorganisms pumping iron: Anaerobic microbial iron oxidation and reduction, *Nat. Rev. Microbiol.*, *4*(10), 752–764.

Wishner, K. F., C. J. Ashjian, C. Gelfman, M. M. Gowing, L. Kann, L. A. Levin, L. S. Mullineaux, and J. Saltzman (1995), Pelagic and benthic ecology of the lower interface of the Eastern Tropical Pacific oxygen minimum zone, *Deep Sea Res., Part I*, *42*(1), 93–115, doi:10.1016/0967-0637(94)00021-J.

Yang, W. H., K. A. Weber, and W. L. Silver (2012), Nitrogen loss from soil through anaerobic ammonium oxidation coupled to iron reduction, *Nat. Geosci.*, *5*(8), 538–541.

Zheng, Y., A. van Geen, R. F. Anderson, J. V. Gardner, and W. E. Dean (2000), Intensification of the northeast pacific oxygen minimum zone during the bölling-alleröd warm period, *Paleoceanography*, *15*(5), 528–536, doi:10.1029/1999PA000473.

Ziebis, W., J. McManus, T. Ferdelman, F. Schmidt-Schierhorn, W. Bach, J. Muratli, K. J. Edwards, and H. Villinger (2012), Interstitial fluid chemistry of sediments underlying the North Atlantic gyre and the influence of subsurface fluid flow, *Earth Planet. Sci. Lett.*, *323–324*, 79–91, doi:10.1016/j.epsl.2012.01.018.